JOURNAL OF MOLECULAR SPECTROSCOPY 115, 88–104 (1986)

High-Resolution Spectroscopy on the $c^1\Pi \leftarrow a^1\Delta$ Transition in NH

W. UBACHS, G. MEYER, J. J. TER MEULEN, AND A. DYMANUS

Fysisch Laboratorium, Katholieke Universiteit Nijmegen Toernooiveld, 6525 ED Nijmegen, The Netherlands

The spectrum of the $c^1\Pi$, $v = 0 \leftarrow a^1\Delta$, $v = 0$ band of the NH molecule at $\lambda = 324$ nm has been investigated under high resolution by laser-induced fluorescence in a molecular beam. From an analysis of the spectra we obtained: the magnetic dipole interaction constants $a_{N,H}$ and the electric quadrupole constants $eQq_{1,2}$ for both electronic states, the improved values for the Λ-doubling constants q_π, q_π^D, and q_π^H for the $c^1\Pi$ state, and rotational constants for both electronic states up to a third-order centrifugal distortion. Also, the Λ-doubling in the $a^1\Delta$ state could be determined. © 1986 Academic Press, Inc.

1. INTRODUCTION

Exactly 50 years ago three groups reported on the $c^1\Pi$, $v = 0 \rightarrow a^1\Delta$, $v = 0$ emission spectrum of NH at $\lambda = 324$ nm (*1–3*). The subsequent analysis yielded the rotational constants for both the $c^1\Pi$ and $a^1\Delta$ states and the Λ-doubling coefficient in the $c^1\Pi$ state. Recently Ramsay and Sarre (*4*) observed the $c^1\Pi$, $v = 0 \rightarrow a^1\Delta$, $v = 1$ band in higher resolution but the Λ doubling in the $a^1\Delta$ state could not be determined. A complete analysis of several vibrational bands of the $d^1\Sigma^+ \rightarrow c^1\Pi$ and $d^1\Sigma^+ \rightarrow b^1\Sigma^+$ systems was performed by Graham and Lew (*5*). Krishnamurty and Narasinham (*6*) observed a breaking off of the rotational structure in the $d^1\Sigma^+$, $v = 0 \rightarrow c^1\Pi$, $v = 0$ band for $J \geqslant 24$ which they attributed to predissociation in the $c^1\Pi$ state. Since the observation of the $b^1\Sigma^+ \rightarrow X^3\Sigma^-$ singlet–triplet transition by Gilles *et al.* (*7*) it is known that the $a^1\Delta$ state in NH lies 12593 cm^{-1} above the ground state $X^3\Sigma^-$. Recently Rohrer and Stuhl (*8*) reported on their observation of emission from the $a^1\Delta$ state to the $X^3\Sigma^-$ ground state at $\lambda = 794$ nm in low resolution.

Over the past years there has been interest in the formation and chemistry of the NH molecule in the metastable $a^1\Delta$ state. In the photolysis of hydrazoic acid NH is produced in the singlet states $a^1\Delta$ and $b^1\Sigma^+$ (*9*, *10*). Piper *et al.* (*11*) applied laser-induced fluorescence (LIF) detection to study the NH($a^1\Delta$) fragments in this photolysis reaction. Chemical reactions involving metastable NH($a^1\Delta$) radicals were also studied (*12*).

In a previous communication we reported observation and analysis of the high-resolution spectrum of the $A^3\Pi$, $v = 0 \leftarrow X^3\Sigma^-$, $v = 0$ transition in NH by laser-induced fluorescence detection in a molecular beam (*13*, *14*).[1] In the present investigation the LIF technique is applied to the $c^1\Pi$, $v = 0 \leftarrow a^1\Delta$, $v = 0$ band. The hyperfine structure in both electronic states $a^1\Delta$ and $c^1\Pi$ could be resolved for the

[1] We regret omitting Ref. (*14*) on the $A^3\Pi$–$X^3\Sigma$ system in our previous work.

0022-2852/86 $3.00

first time, resulting in the determination of the magnetic dipole interaction constants $a_{N,H}$ for both nuclei and the electric quadrupole constants $eQq_{1,2}$ for the nitrogen nucleus. The accuracy in the rotational and Λ-doubling constants in the $c^1\Pi$ state could be further improved by including centrifugal distortion. Absolute frequency measurements of the $c^1\Pi$, $v = 0 \leftarrow a^1\Delta$, $v = 0$ transitions yielded accurate rotational constants up to a third-order centrifugal distortion parameter. From frequency differences in observed Λ splittings in $Q(J)$ transitions on the one hand and $P(J + 1)$ and $R(J - 1)$ transitions on the other hand the very small Λ doubling in the $a^1\Delta$ state could be determined. To our knowledge this represents the first accurate determination of the Λ doubling in a $^1\Delta$ state.

2. EXPERIMENTAL DETAILS

The molecular beam apparatus, the coaxial microwave discharge source for the NH production, and the fluorescence detection zone have been described in detail before (*13*). The optimal production conditions for NH in the metastable $a^1\Delta$ state are nearly the same as for the NH molecules in the electronic ground state. Only the optimal pressure is slightly lower, which is probably due to collisional quenching to the ground electronic state. From relative signal intensities, oscillator strengths (*15*, *16*), and number of fine structure states we estimate that in this production method about 14% of the NH molecules are formed in the $a^1\Delta$ state. In this estimate we also corrected for the fact that the fluorescence in the $c^1\Pi \rightarrow b^1\Sigma^+$ channel, at $\lambda = 450$ nm, which is about 50% according to McDonald *et al.* (*17*), is suppressed by optical filters in the detection zone.

The radiative lifetime of the NH($a^1\Delta$) molecule is long enough to reach the detection zone at a distance of 15 cm from the beam orifice. The molecules could be detected also in a second LIF detection zone at a distance of about 60 cm from the source. The decrease in signal, which is normally caused by beam divergence was not significantly larger than for longer lived species such as NH($X^3\Sigma^-$) and we conclude that the lifetime of the $a^1\Delta$ state is longer than 1 msec. Recently Rohrer and Stuhl (*8*) estimated a lower limit of the radiative lifetime of 30 msec.

The NH molecules in the molecular beam were excited with 2 mW continuous laser power from a frequency doubled ring dye laser. The dominant contribution to the spectral linewidth of 13 MHz comes from Doppler broadening, caused by molecular beam divergence.

3. RESULTS AND ANALYSIS

(A) Observed Spectra

The hyperfine structure in the singlet states of NH originates mainly from interactions of the spin $I_H = \frac{1}{2}$ of the hydrogen nucleus and the spin $I_N = 1$ of the nitrogen nucleus with the electronic orbital angular momentum. A smaller contribution comes from the interaction between the quadrupole moment Q of the nitrogen nucleus and the electric field gradient due to the hydrogen nucleus and the electrons. As in the case of the $A^3\Pi$–$X^3\Sigma^-$ triplet spectra (*13*) the singlet spectra consist of 26 hyperfine components for Q transitions and 22 for P transitions. We analyzed the hyperfine splittings of the $Q(J)$ transitions for $J = 2$ to 7 and $P(J)$ transitions for $J = 2$, 5, and 6 of the

$c^1\Pi$, $v = 0 \leftarrow a^1\Delta$, $v = 0$ band. For the low J values the spectra show largest splittings between hyperfine components. For $J > 7$ the overlap of the hyperfine components is too severe to use them in the determination of the hyperfine structure. A typical spectrum is shown in Fig. 1 for the $P(2)$ transition. The splitting in two groups of hyperfine lines is characteristic for the spectra of the rotational transitions. The Λ doubling splits every rotational state of $a^1\Delta$ and $c^1\Pi$ in positive and negative parity states, so that two transitions are possible. The experimental values of 120 hyperfine splittings, measured relative to the $F'' = J'' + \frac{3}{2} \rightarrow F' = J' + \frac{3}{2}$ components, which are strongest in all spectra, are given in Table I. The quoted experimental errors correspond to 1 SD of at least four measurements for each line, with a minimum of 2 MHz to account for possible systematic errors. The error was increased when overlap occurred for different hyperfine components. In the table the hyperfine components are denoted with the quantum number F of the total angular momentum. In cases where F does not define the energy level unambiguously we introduced an extra index (1) and (2) for the upper and lower level, respectively. In Table II the values of the observed splittings, caused by the Λ doubling are given for 21 rotational transitions up to $J = 16$ as measured in continuous scans of the laser. Only in the case of the $Q(J)$ transitions for $J = 14$ to 16 the splittings were obtained from absolute frequency measurements. Table III gives the absolute frequencies of the rotational transitions.

(B) Hyperfine Structure

The experimental results have been fitted to an effective Hamiltonian for the hyperfine structure in the $a^1\Delta$ and $c^1\Pi$ states. Using the same notation as in the previous paper (*13*) the hyperfine Hamiltonian is

$$H_{\mathrm{hf}} = \sum_{i,k,q} \zeta_k (-)^q T_q^{(1)}(I_k) T_{-q}^{(1)}(l_i)/r_{ik}^3 + \sum_{i,q} (-)^q T_q^{(2)}(Q) T_{-q}^{(2)}(V_i) \tag{1}$$

where the summation i is over all electrons and k over both nuclear spins. The matrix elements were calculated with symmetrized Hund's case (a) basis functions in the coupling scheme $J + I_1 = F_1$, $F_1 + I_2 = F$ ($I_1 = I_{\mathrm{N}}$, $I_2 = I_{\mathrm{H}}$):

$$|^1\Lambda J I_1 F_1 I_2 F M_F \pm\rangle = \frac{1}{\sqrt{2}} \{|\Lambda J I_1 F_1 I_2 F M_F\rangle \pm |-\Lambda J I_1 F_1 I_2 F M_F\rangle\}. \tag{2}$$

The matrix elements for both $a^1\Delta$ ($\Lambda = 2$) and $c^1\Pi$ ($\Lambda = 1$) states are

$$\begin{aligned}
&\langle {}^1\Lambda J I_1 F_1 I_2 F \pm | H_{\mathrm{hf}} | {}^1\Lambda J I_1 F_1' I_2 F \pm \rangle \\
&= \Lambda a_1 (-)^{I_1+F_1+\Lambda} (2J+1) \sqrt{I_1(I_1+1)(2I_1+1)} \begin{pmatrix} J & 1 & J \\ -\Lambda & 0 & \Lambda \end{pmatrix} \begin{Bmatrix} F_1 & I_1 & J \\ 1 & J & I_1 \end{Bmatrix} \delta_{F_1 F_1'} \\
&\quad + \Lambda a_2 (-)^{I_2-I_1+F+\Lambda-1} (2J+1) \sqrt{I_2(I_2+1)(2I_2+1)} \sqrt{(2F_1+1)(2F_1'+1)} \\
&\quad \times \begin{pmatrix} J & 1 & J \\ -\Lambda & 0 & \Lambda \end{pmatrix} \begin{Bmatrix} F_1 & F_1' & 1 \\ J & J & I_1 \end{Bmatrix} \begin{Bmatrix} F_1 & F_1' & 1 \\ I_2 & I_2 & F \end{Bmatrix} \\
&\quad + (-)^{I_1-F_1+\Lambda} (2J+1) \sqrt{\frac{(2I_1+1)(2I_1+2)(2I_1+3)}{2I_1(2I_1-1)}} \begin{Bmatrix} I_1 & I_1 & 2 \\ J & J & F_1 \end{Bmatrix} \delta_{F_1 F_1'} \\
&\quad \times \left[\frac{eQq_1}{4} \begin{pmatrix} J & 2 & J \\ -\Lambda & 0 & \Lambda \end{pmatrix} \pm \frac{eQq_2}{4} \begin{pmatrix} J & 2 & J \\ -\Lambda & 2 & -\Lambda \end{pmatrix} \delta_{\Lambda,1} \right].
\end{aligned} \tag{3}$$

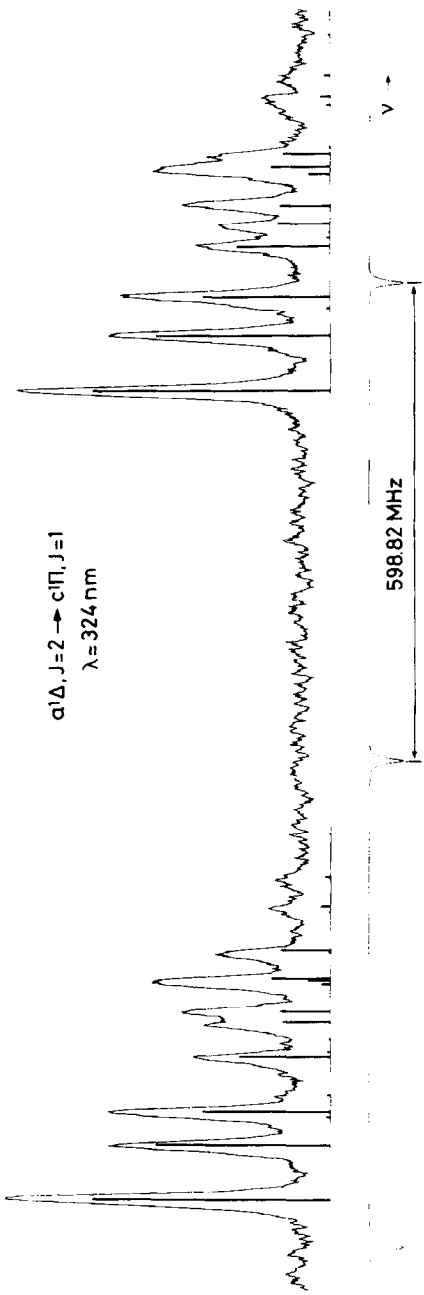

FIG. 1. Observed spectrum of the $P(2)$ transition. The stick spectrum represents calculated energy splittings and relative line intensities.

TABLE I

Observed Hyperfine Splittings (in MHz) for NH in $c^1\Pi$, $v = 0 \leftarrow a^1\Delta$, $v = 0$ Transitions and Deviations from a Least-Squares Fit

F'' → F'	Obs. Freq	Obs.-Calc.	Obs. Freq.	Obs.-Calc.
Transition Q(2)	upper Λ-doublet		lower Λ-doublet	
$7/2 \rightarrow 5/2_2$	-58.3 ± 3.5	0.8	-49.1 ± 3.5	0.1
$5/2_1 \rightarrow 3/2_1$	27.6 ± 3.5	0.7	35.1 ± 4.5	-0.2
$5/2_1 \rightarrow 5/2_1$	79.3 ± 2.5	-0.6	80.2 ± 2.5	0.0
$5/2_2 \rightarrow 3/2_2$	139.8 ± 3.5	0.7	136.2 ± 3.0	1.0
$5/2_2 \rightarrow 5/2_2$	172.8 ± 3.0	0.0	182.2 ± 2.0	-0.5
$3/2_1 \rightarrow 3/2_1$	230.9 ± 4.5	0.1	235.2 ± 4.0	-4.1
$3/2_2 \rightarrow 1/2$	283.4 ± 5.5	-1.5	279.9 ± 4.5	0.7
$3/2_2 \rightarrow 3/2_2$	301.4 ± 5.5	-1.7	297.2 ± 4.5	-2.0
$3/2_2 \rightarrow 5/2_2$	334.9 ± 3.5	-2.0	344.1 ± 4.5	-2.7
$1/2 \rightarrow 1/2$	371.4 ± 5.0	-1.6	365.4 ± 4.5	-1.9
$1/2 \rightarrow 3/2_2$	389.5 ± 5.0	-1.7	385.2 ± 5.0	-2.1
Transition Q(3)				
$9/2 \rightarrow 7/2_2$	-39.0 ± 3.0	0.0	-26.8 ± 4.0	1.9
$7/2_1 \rightarrow 5/2_1$	25.3 ± 4.0	2.7	35.2 ± 3.5	2.8
$7/2_1 \rightarrow 7/2_1$	59.6 ± 2.5	0.3	60.4 ± 3.0	0.7
$7/2_2 \rightarrow 5/2_2$	90.7 ± 4.5	1.5	88.6 ± 3.5	2.3
$7/2_2 \rightarrow 7/2_2$	113.5 ± 3.0	-0.1	123.6 ± 3.5	-0.3
$7/2_2 \rightarrow 9/2$			154.4 ± 3.5	1.8
$5/2_1 \rightarrow 5/2_1$	162.0 ± 2.5	-2.4	174.2 ± 4.0	0.0
$5/2_2 \rightarrow 5/2_2$	204.1 ± 3.5	0.1	201.8 ± 3.5	0.7
$5/2_2 \rightarrow 7/2_2$	229.9 ± 4.0	1.5	238.5 ± 4.5	-0.2
$3/2 \rightarrow 3/2$	258.9 ± 3.0	-0.8	257.3 ± 3.0	1.3
$3/2 \rightarrow 5/2_2$	276.0 ± 3.5	1.5	272.1 ± 4.0	0.5
$3/2 \rightarrow 5/2_1$			293.2 ± 6.0	-1.8
Transition Q(4)	upper Λ-doublet		lower Λ-doublet	
$11/2 \rightarrow 9/2_2$	-27.1 ± 5.5	2.1	-14.4 ± 6.0	4.3
$9/2_1 \rightarrow 9/2_1$	46.9 ± 2.5	-0.2	47.8 ± 2.5	0.3
$9/2_2 \rightarrow 7/2_2$	69.6 ± 5.5	3.9		
$9/2_2 \rightarrow 9/2_2$	84.4 ± 4.0	-0.5	95.9 ± 2.5	0.6
$9/2_2 \rightarrow 11/2$	116.7 ± 5.5	2.6		
$7/2_1 \rightarrow 7/2_1$	126.5 ± 4.0	-1.3	141.4 ± 4.0	3.2
$7/2_2 \rightarrow 7/2_2$	155.1 ± 4.0	0.6	156.7 ± 4.0	4.5
$7/2_2 \rightarrow 9/2_2$	175.0 ± 4.5	1.4	185.6 ± 6.0	1.5
$5/2 \rightarrow 5/2$	200.6 ± 3.5	0.7	200.9 ± 4.5	3.8
$5/2 \rightarrow 7/2_1$	218.9 ± 6.0	-0.7		
Transition Q(5)				
$11/2_1 \rightarrow 11/2_1$	39.1 ± 3.5	0.2	39.5 ± 3.0	0.0
$11/2_2 \rightarrow 11/2_2$	67.0 ± 3.0	-0.8	80.8 ± 3.0	2.5
$9/2_1 \rightarrow 9/2_1$	104.4 ± 3.5	-0.1	119.2 ± 4.5	b
$9/2_2 \rightarrow 9/2_2$	125.7 ± 3.0	1.0		
$7/2 \rightarrow 7/2$	164.3 ± 3.0	1.6	162.9 ± 4.5	2.4
Transition Q(6)				
$13/2_1 \rightarrow 13/2_1$	33.8 ± 4.0	0.6	33.6 ± 2.5	-0.7
$13/2_2 \rightarrow 13/2_2$	57.3 ± 4.0	0.7	68.9 ± 2.5	2.2
$11/2_1 \rightarrow 11/2_1$	90.3 ± 4.5	1.9	102.5 ± 5.5	b
$11/2_2 \rightarrow 11/2_2$	109.2 ± 4.5	4.6		
$9/2 \rightarrow 9/2$	142.4 ± 6.0	5.1	138.6 ± 3.5	3.2

TABLE I—*Continued*

F" → F'	Obs. Freq	Obs.-Calc.	Obs. Freq.	Obs.-Calc.
Transition Q(7)	upper Λ-doublet		lower Λ-doublet	
$15/2_1 \rightarrow 15/2_1$	29.1 ± 5.0	0.2	28.8 ± 5.0	-2.2
$15/2_2 \rightarrow 15/2_2$	48.6 ± 5.5	-0.1	61.2 ± 5.0	3.4
$13/2_1 \rightarrow 13/2_1$	77.8 ± 5.5	1.2	90.7 ± 5.0	b
$13/2_2 \rightarrow 13/2_2$	93.5 ± 5.5	3.3		
$11/2 \rightarrow 11/2$	121.9 ± 5.0	3.1	122.6 ± 5.0	5.4
Transition P(2)				
$5/2_1 \rightarrow 3/2_1$	67.6 ± 3.0	-0.6	69.2 ± 2.5	0.7
$5/2_2 \rightarrow 3/2_2$	108.2 ± 3.0	-0.5	118.1 ± 2.5	0.1
$3/2_1 \rightarrow 1/2_1$	175.3 ± 3.0	-0.5	181.8 ± 4.0	0.9
$3/2_2 \rightarrow 1/2_2$	215.7 ± 6.0	-3.7	207.9 ± 4.0	-1.6
$5/2_2 \rightarrow 5/2$	231.8 ± 5.5	-0.1	233.7 ± 4.0	1.8
$3/2_2 \rightarrow 3/2_2$	270.2 ± 5.5	-2.6	278.8 ± 3.5	-3.2
$1/2 \rightarrow 1/2_2$	302.9 ± 4.5	-4.6	296.5 ± 4.5	-1.1
$1/2 \rightarrow 3/2_2$	359.9 ± 5.5	-1.0	369.5 ± 4.5	-0.6
$3/2_2 \rightarrow 5/2$	394.5 ± 6.0	-1.5	396.4 ± 6.0	0.4
Transition P(5)				
$11/2_1 \rightarrow 9/2_1$	36.6 ± 4.0	-0.1	35.7 ± 2.5	-1.4
$11/2_2 \rightarrow 9/2_2$	61.5 ± 4.0	-0.6	72.0 ± 2.5	-0.6
$9/2_1 \rightarrow 7/2_1$	96.8 ± 4.0	-0.3	109.9 ± 4.0	b
$9/2_2 \rightarrow 7/2_2$	116.6 ± 4.0	1.1		
$7/2 \rightarrow 5/2$	152.0 ± 4.0	0.4	150.9 ± 3.5	2.1
Transition P(6)				
$13/2_1 \rightarrow 11/2_1$	30.2 ± 3.5	-1.4	32.9 ± 3.5	0.7
$13/2_2 \rightarrow 11/2_2$	52.9 ± 4.0	0.0	64.1 ± 3.5	0.7
$11/2_1 \rightarrow 9/2_1$	86.3 ± 3.5	3.0	97.6 ± 5.0	b
$11/2_2 \rightarrow 9/2_2$	100.8 ± 3.5	2.4		
$9/2 \rightarrow 7/2$	132.9 ± 4.0	3.2	131.6 ± 4.5	4.2

Note. The splittings are relative to the $F'' = J'' + \frac{3}{2} \rightarrow F' = J' + \frac{3}{2}$ hyperfine component. The quantum numbers F'' and F' refer to the $a^1\Delta$ and $c^1\Pi$ states, while the indices (1) and (2) denote upper and lower energy levels in cases where F is not uniquely defining a hyperfine state. The lines marked with *b* were not taken into the data set of the computer program because of severe overlap.

The constants a_k are the magnetic hyperfine coupling constants of Frosch and Foley (*18*) for both nuclei and q_1 and q_2 are the quadrupole coupling constants for the nitrogen nucleus.

As can be seen from Fig. 1 there is clearly a difference between the hyperfine splittings of $+ \leftarrow -$ and $- \leftarrow +$ Λ-doublet transitions. The last term in Eq. (3), that corresponds to the $\Delta\Lambda = \pm 2$ coupling between the states, is responsible for this difference in hyperfine structure for levels with opposite symmetry in the Hund's case (a) wave function in the $c^1\Pi$ state. Both Λ-doublet levels in each rotational state of $a^1\Delta$ have the same hyperfine structure.

The energy matrix was first diagonalized with estimated values for the constants. With a proper set of constants all 120 hyperfine components could be identified from

TABLE II

Observed Splittings (in MHz) in $c^1\Pi$, $v = 0 \leftarrow a^1\Delta$, $v = 0$ Transitions

Transition	Observed	$\Delta E_\pi(J)_{obs}$	$\Delta E_\pi(J)_{obs} - \Delta E_\pi(J)_{calc}$
P(2)	1005 (10)	1005	1
Q(2)	3007 (10)	3007	-2
Q(3)	5995 (15)	5996	-11
Q(4)	9997 (10)	9999	9
P(5)	9989 (20)	9985	-5
Q(5)	14969 (50)	14973	26
P(6)	14987 (20)	14979	32
Q(6)	20939 (135)	20947	85
Q(7)	27686 (20)	27701	-18
Q(8)	35461 (20)	35485	-16
P(9)	35534 (20)	35496	-5
Q(9)	44152 (15)	44168	-19
R(8)	44214 (20)	44190	3
P(10)	44247 (20)	44190	3
Q(10)	53710 (15)	53767	5
P(11)	53849 (10)	53766	4
Q(11)	64127 (15)	64200	-4
P(12)	64325 (10)	64209	5
Q(14)	100362 (70)	100573	-23
Q(15)	114014 (70)	114289	-90
Q(16)	128683 (70)	129037	51

Note. The column $\Delta E_\pi(J)_{obs}$ gives the Λ-doublet splittings in the $c^1\Pi$ state as obtained from the values in the second column and the Λ doubling in the $a^1\Delta$ state. The error is 1 SD from at least four measurements. In the last column the deviations from a least-squares fit are given.

calculated splittings and relative line intensities. After the assignment of the hyperfine transitions the constants were obtained in a least-squares fit by computer; they are listed in Table IV. The agreement between calculated splittings and observed data is very good as illustrated in Fig. 1. for the $P(2)$ transition. The deviations between calculated and measured splittings are given in Table I and are smaller than the experimental error. The observed line intensities of the strongest components is somewhat too low relative to the weak components, which is probably due to saturation.

The hyperfine constants can be interpreted in terms of expectation values of electron densities as given in Ref. (*13*):

$$a_k = 2g_k\mu_B\mu_N\langle 1/r_{ik}^3\rangle_\pi \tag{4}$$

$$q_1 = (2/R_{NH}^3) - \langle(3\cos^2\Theta_{1N} - 1)/r_N^3\rangle_T \tag{5}$$

$$q_2 = -3\langle(\sin^2\Theta_{1N})/r_N^3\rangle_T. \tag{6}$$

The electron densities around the N and H nuclei in the $a^1\Delta$, $A^3\Pi$, and $c^1\Pi$ states calculated from the hyperfine constants in Ref. (*13*) and the present experiment are listed in Table V.

The molecular orbital (MO) configuration for the $a^1\Delta$ state is $(1s\sigma)^2 \times (2s\sigma)^2(2p\sigma)^2(2p\pi)^2$, the same as for the ground electronic state $X^3\Sigma^-$. The $c^1\Pi$ state arises from the same MO configuration as the $A^3\Pi$ state, namely, $(1s\sigma)^2(2s\sigma)^2(2p\sigma)(2p\pi)^3$. Only π electrons contribute to the a constant and it is not surprising that the average values for $1/r^3$ in the three electronic states are nearly equal.

TABLE III

Absolute Frequencies (in cm^{-1}) for Transitions $c^1\Pi$, $v = 0 \leftarrow a^1\Delta$, $v = 0$ in NH and Deviations from a Least-Squares Fit

J	P-transition	obs.-calc.	Q-transition	obs.-calc.
2	30685.3882(35)	-0.0021	30741.9716(20)	-0.0004
	685.3549(35)	-0.0020	741.8714(20)	-0.0002
3			30728.2197(20)	0.0010
			728.0203(20)	0.0020
4			30709.8154(20)	-0.0017
			709.4823(20)	-0.0016
5	30546.1970(20)	0.0010	30686.7138(60)	0.0025
	545.8640(20)	0.0014	686.2159(60)	0.0030
6	30490.8030(20)	-0.0009	30658.8307(20)	0.0011
	490.3040(20)	-0.0011	658.1355(20)	0.0015
7			30626.0825(50)	-0.0014
			625.1590(50)	-0.0007
8			30588.3627(55)	-0.0054
			587.1812(50)	-0.0036
9	30297.1853(40)	0.0025	30545.5558(35)	-0.0011
	295.9994(40)	0.0020	544.0838(35)	-0.0004
10	30223.2662(20)	-0.0004	30497.5024(50)	-0.0014
	221.7903(20)	-0.0005	495.7093(50)	-0.0031
11			30444.0424(40)	0.0029
			441.9028(40)	0.0021
12	30060.7432(20)	-0.0011		
	058.6001(20)	0.0013		
14			30249.1117(20)	-0.0005
			245.7640(20)	0.0004
15			30171.7448(20)	-0.0016
			167.9417(20)	0.0015
16			30087.6423(20)	0.0007
			083.3499(20)	-0.0007

TABLE IV

Hyperfine Constants for the $a^1\Delta$, $v = 0$ and $c^1\Pi$, $v = 0$ States of the NH Molecule (in MHz)

	$c^1\Pi$	$a^1\Delta$	$A^3\Pi$
a_N	106.3 ± 1.8	110.0 ± 0.5	89.6 ± 2.3
$eQq_{1,N}$	11.4 ± 2.3	-8.0 ± 2.6	7.1 ± 1.5
$eQq_{2,N}$	-32.0 ± 3.2		21.9 ± 2.4
a_H	58.2 ± 4.3	69.6 ± 1.2	74.1 ± 1.5

Note. The subscripts N and H refer to the nitrogen and hydrogen nuclei. For comparison the values of these constants in the $A^3\Pi$ state also are given (*13*).

TABLE V

Averaged Electron Densities around the N and H Nuclei in the $a^1\Delta$, $c^1\Pi$, and $A^3\Pi$, $v = 0$ States of the NH Molecule (in Units of 10^{-30} m^{-3})

	$c^1\Pi$	$a^1\Delta$	$A^3\Pi$
$\langle 1/r_H^3 \rangle_\pi$	0.74 (5)	0.88 (2)	0.94 (5)
$\langle 1/r_N^3 \rangle_\pi$	17.1 (3)	17.7 (1)	14.4 (4)
$\langle (3\cos^2\theta_N - 1)/r_N^3 \rangle_T$	-18.3 (40)	-12.0 (45)	-10.2 (23)
$\langle \sin^2\theta_N/r_N^3 \rangle_T$	18.4 (18)		-12.7 (15)

In the spectroscopic approximation the expression for q_2 can be rewritten in terms of the unpaired open shell electrons if the proper sign is taken. In the previous paper this is done for the $A^3\Pi$ state by expressing the electronic wave functions in Slater determinants. An analogous procedure can be followed for the $c^1\Pi$ state. The $|\Lambda = +1, \Sigma = 0\rangle$ Slater determinant wave function in the $c^1\Pi$ state is chosen orthogonal to the $|\Lambda = +1, \Sigma = 0\rangle$ state of the $A^3\Pi$ multiplet (*13*):

$$|\Lambda = +1, \Sigma = 0\rangle = \sqrt{1/2}[\{\sigma^-\pi_+^-\pi_+^+\pi_-^+\} - \{\sigma^+\pi_+^-\pi_+^+\pi_-^-\}]$$

$$|\Lambda = -1, \Sigma = 0\rangle = \sqrt{1/2}[\{\sigma^-\pi_-^-\pi_-^+\pi_+^+\} - \{\sigma^+\pi_-^-\pi_-^+\pi_+^-\}]. \quad (7)$$

Using these Slater determinants we calculated the expectation values for the quadrupole tensor elements in the $c^1\Pi$ state[2]:

$$\begin{aligned} q_2 &= \frac{2\sqrt{6}}{e}\langle \Lambda = 1, \Sigma = 0|T_2^{(2)}(V)|\Lambda = -1, \Sigma = 0\rangle \\ &= -\frac{\sqrt{6}}{e}(\langle\{\sigma^-\pi_+^-\pi_+^+\pi_-^+\}|T_2^{(2)}(V)|\{\sigma^-\pi_-^-\pi_-^+\pi_+^+\}\rangle \\ &\quad + \langle\{\sigma^+\pi_+^-\pi_+^+\pi_-^-\}|T_2^{(2)}(V)|\{\sigma^+\pi_+^-\pi_-^+\pi_-^-\}\rangle) \\ &= \sqrt{6}[\langle\pi_+^-|C_2^{(2)}(\Theta_{1N}, \phi_{1N})/r_{1N}^3|\pi_-^-\rangle + \langle\pi_+^+|C_2^{(2)}(\Theta_{1N}, \phi_{1N})/r_{1N}^3|\pi_-^+\rangle] \\ &= -3\langle\sin^2\Theta_{1N}/r_{1N}^3\rangle_u. \end{aligned} \quad (8)$$

So when the expectation value of $\sin^2\Theta_{1N}/r_{1N}^3$ is calculated for the unpaired electrons the same result is obtained as for the total electron contribution [Eq. (6)]. This is not the case for the $A^3\Pi$ state, where the expectation values for the unpaired and total electron distribution differ in sign (*13*). Consequently a positive value for q_2 was obtained for $A^3\Pi$, whereas a negative value is found for the $c^1\Pi$ state. The difference between the absolute values for q_2 in the $A^3\Pi$ and $c^1\Pi$ states is not significant in view of the limited validity of the spectroscopic approximation.

[2] In Appendix A of (*13*) some typing errors are present: $T_2^{(2)}$ and $T_{-1}^{(1)}$ have to be $T_2^{(2)}$ and $T_1^{(1)}$, respectively whereas the factor of -3 in front of $\langle\pi_+^-|C_2^{(2)}(\Theta_{1N}, \phi_{1N})/r_{1N}^3|\pi_-^-\rangle$ must be $-2\sqrt{6}$.

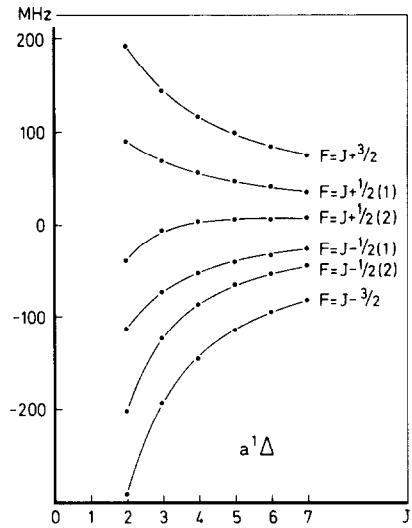

FIG. 2. Calculated hyperfine energy levels, relative to the unperturbed rotational state J, in the $a^1\Delta$ state. Because there is no contribution of the symmetry dependent eQq_2 matrix elements to the hyperfine structure in the $a^1\Delta$, the hyperfine energy splittings in both upper and lower Λ-doublet states are the same.

The same conclusion holds for the q_1 constant. We experimentally find a negative q_1 for the $a^1\Delta$ state. Also for the $X^3\Sigma^-$ state, having the same MO configuration, a negative value was obtained for q_1.

Because of the fact that the measured hyperfine splittings are sums and differences of hyperfine energy levels, they give no direct insight into the hyperfine structure of both states. We plotted the hyperfine energy levels relative to the unperturbed rotational state J for the $a^1\Delta$ state in Fig. 2 and for both Λ-doublet states of the $c^1\Pi$ state in Fig. 3.

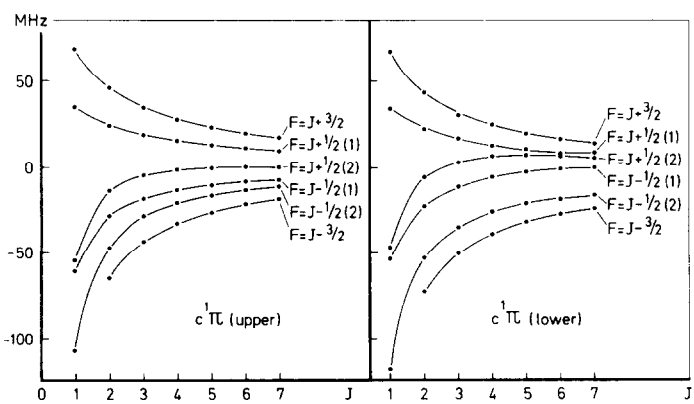

FIG. 3. Calculated hyperfine energy levels, for upper and lower Λ-doublet states in the $c^1\Pi$ state.

(C) Lambda Doubling

The values of the Λ splittings were obtained from the separation between the $F'' = J'' + \frac{3}{2} \rightarrow F' = J' + \frac{3}{2}$ hyperfine components in both parity transitions. The results of the observed splittings as listed in Table II are the sum of (in case of P or R transitions) or difference between (in case of Q transitions) the Λ-doublet splittings in the initial $a^1\Delta$ and final $c^1\Pi$ state. The values are corrected for the small difference ($\leqslant 4$ MHz) in hyperfine energy of the $F' = J' + \frac{3}{2}$ level in both Λ-doublet states of the $c^1\Pi$ state. For transitions originating from higher J states ($J > 7$) the hyperfine structure was unresolved, and therefore no corrections were made.

The Λ doubling in the $^1\Pi$ and $^1\Delta$ states is caused by the interaction Hamiltonian

$$V = -B(J_+L_- + J_-L_+) \tag{9}$$

connecting states with $\Delta\Lambda = \pm 1$. The matrix elements between $^1\Delta$ and $^1\Pi$, $\langle {}^1\Delta JM_J\pm|V|{}^1\Pi JM_J\pm\rangle$, are nonzero but equal for both symmetric and antisymmetric states. Consequently the Λ doubling has to be caused by a second-order coupling with the nearby $b^1\Sigma^+$ state and the higher $d^1\Sigma^+$ state. The antisymmetric $^1\Delta$ state is unaffected by the interacting $^1\Sigma^+$ states because the matrix elements between opposite symmetries are zero. From third-order perturbation theory it follows that the symmetric state is shifted downward in energy by

$$\Delta E_\Delta = |q_\Delta|(J-1)J(J+1)(J+2) \tag{10}$$

with q_Δ the Λ-doubling parameter:

$$q_\Delta = 2\frac{|\langle {}^1\Delta_2|BL_+|{}^1\Pi_1\rangle|^2}{(E_\Delta - E_\pi)^2}\left[\frac{|\langle {}^1\Pi_1|BL_+|b^1\Sigma^+\rangle|^2}{(E_\Delta - E_{b\Sigma})} + \frac{|\langle {}^1\Pi_1|BL_+|d^1\Sigma^+\rangle|^2}{(E_\Delta - E_{d\Sigma})}\right]. \tag{11}$$

Consequently the Λ-doubling in the $a^1\Delta$ state is much smaller than in the $c^1\Pi$ state where it is caused by a first-order interaction with $^1\Sigma$ states. Ramsay and Sarre (*4*) extended the expression for the Λ-doublet splitting in the $c^1\Pi$ state with a centrifugal distortion term. For the present analysis we need an expression for ΔE_π which includes centrifugal distortion up to a third order:

$$\Delta E_\pi(J) = q_\pi J(J+1) + q_\pi^D J^2(J+1)^2 + q_\pi^H J^3(J+1)^3 \tag{12}$$

with

$$q_\pi = 2\left[\frac{|\langle {}^1\Pi_1|BL_+|b^1\Sigma^+\rangle|^2}{(E_\pi - E_{b\Sigma})} + \frac{|\langle {}^1\Pi_1|BL_+|d^1\Sigma^+\rangle|^2}{(E_\pi - E_{d\Sigma})}\right] \tag{13}$$

and q_π^D and q_π^H the centrifugal distortion parameters.

The $b^1\Sigma^+$ state, lying 22121 cm^{-1} below the $c^1\Pi$ state causes an upward shift of the symmetric $c^1\Pi$ levels, whereas the $d^1\Sigma^+$ state at 39512 cm^{-1} above the $c^1\Pi$ state causes a downward shift of the same levels. The antisymmetric $c^1\Pi$ is unaffected. In an analysis of the $c^1\Pi \rightarrow b^1\Sigma^+$ band system Whittaker (*19*) showed that the interaction of the $b^1\Sigma^+$ state is stronger and therefore the upper Λ-doublet levels of the $c^1\Pi$ state have positive symmetry for the electronic part of the wave function.

The parities of the upper and lower Λ-doublet states in both $c^1\Pi$ and $a^1\Delta$ do not follow straightforwardly from a rotational analysis of the $c^1\Pi \leftarrow a^1\Delta$ transition, because

both states split in positive and negative parity states, thus allowing for two possible $+ \leftrightarrow -$ transitions. The situation is different for transitions to $^1\Sigma^+$ or $^1\Sigma^-$ states from which the parities in the $c^1\Pi$ state can be determined. In their analysis of the $d^1\Sigma^+$–$c^1\Pi$ and $c^1\Pi$–$b^1\Sigma^+$ transitions Lunt *et al.* (*20, 21*) showed that the parities in the $c^1\Pi$ state are $(-)^J$ for the upper Λ-doublet state and $(-)^{J+1}$ for the lower state. From the fact that observed splittings in $P(J + 1)$ transitions are larger than in $Q(J)$ transitions (Table II), we deduce: parity $(-)^{J+1}$ for the upper Λ-doublet state and $(-)^J$ for the lower one in the $a^1\Delta$ state. Application of the reflection operator σ_{xz} to the symmetrized wavefunctions with the reflection symmetry of the electronic part derived in the Slater determinant formalism as described in Appendix A of Ref. (*13*)

$$\sigma_{xz}|^1\Pi JM_J\pm\rangle = \pm(-)^J|^1\Pi JM_J\pm\rangle$$
$$\sigma_{xz}|^1\Delta JM_J\pm\rangle = \pm(-)^J|^1\Delta JM_J\pm\rangle \qquad (14)$$

gives a relation between the parity of the state and the symmetry of the corresponding wave function. It follows that the upper Λ-doublet state in $c^1\Pi$ and the lower one in $a^1\Delta$ corresponds to a symmetric wave function. This is in agreement with Eq. (13), an upward shift in the $c^1\Pi$ state, and with Eq. (11), a downward shift in the $a^1\Delta$ state, for the symmetric wave functions. Furthermore in the analysis of the hyperfine structure, where matrix elements for the eQq_2 interaction yield different contributions for symmetric and antisymmetric states in $c^1\Pi$, the sign of the q_2 constant is obtained correctly only if the upper Λ-doublet states in $c^1\Pi$ are of positive symmetry.

In Fig. 4 it is shown how the observed splittings in $P(J + 1)$ transitions [i.e., $\Delta\nu_P(J + 1)$] and $Q(J)$ transitions [i.e., $\Delta\nu_Q(J)$] can be evaluated in terms of sums and

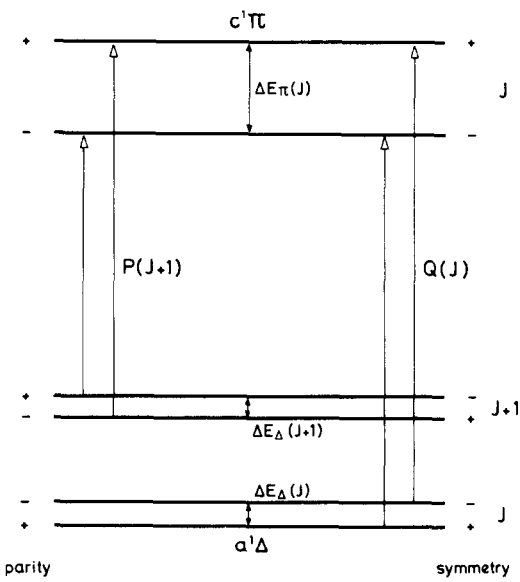

FIG. 4. Scheme (not to scale) of transitions between upper and lower Λ-doublet states in $c^1\Pi$ and $a^1\Delta$. The parity is an alternating quantity in J and should be multiplied by $(-1)^J$.

differences of Λ-doubling energies $\Delta E_\pi(J)$ and $\Delta E_\Delta(J)$ in the $c^1\Pi$ and $a^1\Delta$ state, respectively:

$$\Delta\nu_P(J+1) = \Delta E_\pi(J) + \Delta E_\Delta(J+1)$$

$$\Delta\nu_Q(J) = \Delta E_\pi(J) - \Delta E_\Delta(J). \tag{15}$$

It follows that

$$\Delta E_\Delta(J) + \Delta E_\Delta(J+1) = \Delta\nu_P(J+1) - \Delta\nu_Q(J). \tag{16}$$

There is an analogous relation for the differences of the splittings in $R(J)$ and $Q(J+1)$ transitions:

$$\Delta E_\Delta(J) + \Delta E_\Delta(J+1) = \Delta\nu_R(J) - \Delta\nu_Q(J+1). \tag{17}$$

According to Eq. (10) this sum of Λ-doublet energies in the $a^1\Delta$ state is related to the Λ-doubling constant q_Δ by

$$\Delta E_\Delta(J) + \Delta E_\Delta(J+1) = |q_\Delta|2J(J+1)^2(J+2). \tag{18}$$

The observed frequency differences from Eqs. (16) and (17) are plotted in Fig. 5 as a function of $2J(J+1)^2(J+2)$. The deviations from a straight line are well within the experimental errors. From a least-squares fit we obtained for the Λ-doubling parameter in the $a^1\Delta$, $v = 0$ state the value $q_\Delta = -4.82 \pm 0.31$ kHz.

From the values in Table IV the Λ-doubling in the $c^1\Pi$ state also was obtained. After correction for the Λ doubling in $a^1\Delta$ the values were fitted to Eq. (12) resulting in the Λ-doubling constants that are presented in Table VI. The present values are in agreement with the results of Ramsay and Sarre (*4*) within their quoted errors.

No ab initio calculations of the Λ-doubling constants in $c^1\Pi$ and $a^1\Delta$ are available. Whittaker (*19*) has calculated q_π in the pure precession approximation. In the assumption that

$$|\langle {}^1\Pi_1|BL_+|b^1\Sigma^+\rangle|^2 = |\langle {}^1\Pi_1|BL_+|d^1\Sigma^+\rangle|^2 = 2B_\Pi^2$$

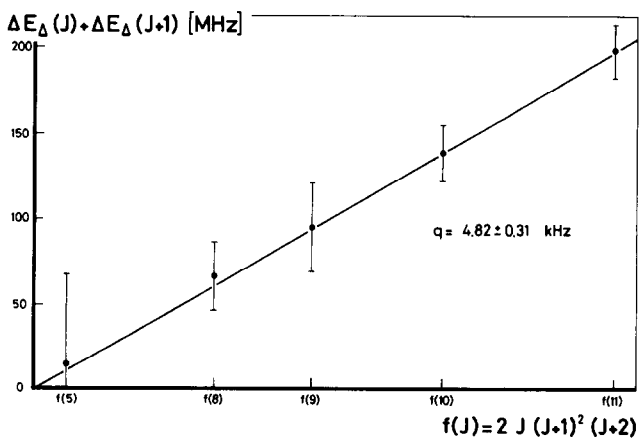

FIG. 5. Sum of Λ-doublet splittings in $a^1\Delta$ for two succesive J states as a function of $2J(J+1)^2(J+2)$.

TABLE VI

Λ-Doubling Constants for the $a^1\Delta$, $v = 0$ and $c^1\Pi$, $v = 0$ States of NH

	present values	Ramsay and Sarre (4)
q_π	502.2 ± 0.3 MHz	498.2 ± 5.4 MHz
q_π^D	- 0.136 ± 0.004 MHz	- 0.084 ± 0.027 MHz
q_π^H	0.121 ± 0.013 kHz	
q_Δ	-4.82 ± 0.31 kHz	

he obtained the value $q_\pi = 477.3$ MHz which is surprisingly close to the experimental value. In this approximation Eqs. (11) and (13) give the relation between q_π and q_Δ:

$$q_\Delta = q_\pi \left(\frac{B_\Delta}{B_\pi}\right)^2 \frac{|\langle {}^1\Delta_2|BL_+|{}^1\Pi_1\rangle|^2}{(E_\Delta - E_\pi)^2} \left[\frac{(E_\Delta - E_{b\Sigma})^{-1} + (E_\Delta - E_{d\Sigma})^{-1}}{(E_\pi - E_{b\Sigma})^{-1} + (E_\pi - E_{d\Sigma})^{-1}}\right]. \tag{19}$$

The matrix elements of BL_+ can be evaluated in terms of determinantal wavefunctions. With the expression (7) for the ${}^1\Pi_1$ wavefunction and

$$|\Lambda = 2, \Sigma = 0\rangle = \{\sigma^+\sigma^-\pi_+^-\pi_+^+\} \tag{20}$$

the pure precession approximation gives

$$\langle {}^1\Delta_2|BL_+|{}^1\Pi_1\rangle = \frac{1}{\sqrt{2}}\left[\langle\sigma^+|B1_+|\pi_-^+\rangle + \langle\sigma^-|B1_+|\pi_-^-\rangle\right]$$

$$= 2B \tag{21}$$

where 1_+ is the single electron operator as applied in Appendix A of Ref. (*13*). Substituting for B the value in the $a^1\Delta$ state we obtain

$$q_\Delta = -1.06 \times 10^{-5} \times q_\pi = -5.36 \text{ kHz}$$

which is not far off from the experimental value.

(D) Rotational Structure

Absolute frequency measurements were performed in order to determine the rotational constants and the centrifugal distortions in the $a^1\Delta$, $v = 0$, and $c^1\Pi$, $v = 0$ states. The absolute frequencies were obtained from a simultaneous recording of the UV spectrum of NH and the absorption of the fundamental laser frequency at $\lambda = 658$ nm in an iodine cell. For several rotational transitions frequency differences of the strongest hyperfine component of both parity transitions to the adjacent I_2-absorption lines were measured in units of markers of our stabilized interferometer. For the higher J transitions, where the hyperfine structure could not be resolved the geometrical center of the transition was determined. The estimated error in every measurement is 60 MHz or larger, due to the drift of the interferometer and in particular to the inaccuracy in the determination of the center of the broad and not always symmetric iodine lines. The corrections to the wavelengths in the I_2 atlas (*22*, *23*) of -0.0056 cm^{-1} were taken into account. In Table III the absolute frequencies of the

observed $c^1\Pi$, $v = 0 \leftarrow a^1\Delta$, $v = 0$ transitions are given. The measurements for transitions from the lower J levels are already corrected for the difference in hyperfine splitting in both $c^1\Pi$ and $a^1\Delta$ states.

For the rotational energies in the $c^1\Pi$ and $a^1\Delta$ states the following expressions are used:

$$E_\Delta = B_\Delta[J(J+1) - 4] - D_\Delta[J(J+1) - 4]^2 + H_\Delta[J(J+1) - 4]^3 - L_\Delta[J(J+1) - 4]^4 + \delta_{S,A} q_\Delta (J-1)J(J+1)(J+2) \quad (22)$$

$$E_\pi = \nu_{00} + B_\pi[J(J+1) - 1] - D_\pi[J(J+1) - 1]^2 + H_\pi[J(J+1) - 1]^3 - L_\pi[J(J+1) - 1]^4 + \delta_{S,A}[q_\pi J(J+1) + q_\pi^D J^2(J+1)^2 + q_\pi^H J^3(J+1)^3]. \quad (23)$$

In these expressions, with $\delta_{S,A} = 1$ for symmetic and 0 for antisymetric states, it is assumed that only symmetric states are shifted by the Λ doubling, in contrast to Ramsay and Sarre (*4*). In a least-squares fit the experimental absolute frequencies were compared to Eqs. (22) and (23) where the values for q_π, q_π^D, q_π^H, and q_Δ as given in Table V were substituted. The resulting values for the rotational constants are listed in Table VII.

The deviations between measured and calculated values are in most cases smaller then the stated experimental errors, which indicates that Eqs. (22) and (23) are good representations for the data and that the experimental error in the absolute frequency, determined relative to the I_2 standard, is smaller than 60 MHz. The calculated error in the rotational constants is roughly a factor of 4 smaller than the error in the best-known values as given by Ramsay and Sarre (*4*), who also incorporated the data of Pearse (*1*) in their analysis. The new values for the $a^1\Delta$ state lie within the error limits of the old values for the rotational constants. For the $c^1\Pi$ state, we find deviations

TABLE VII

Rotational Constants (in cm^{-1}) for the $a^1\Delta$, $v = 0$ and $c^1\Pi$, $v = 0$ States of NH

	present values	Ramsay and Sarre (4)
ν_{00}	30704.0743 (32)	30704.1010 (260)
B_Δ	16.43197 (20)	16.43203 (90)
D_Δ	1.6657 (26) $\times 10^{-3}$	1.6718 (50) $\times 10^{-3}$
H_Δ	0.887 (99) $\times 10^{-7}$	1.207 (400) $\times 10^{-7}$
L_Δ	1.141 (89) $\times 10^{-10}$	
B_π	14.14203 (22)	14.14982 (110)
D_π	2.2220 (27) $\times 10^{-3}$	2.2208 (100) $\times 10^{-3}$
H_π	- 2.061 (94) $\times 10^{-7}$	- 2.075 (260) $\times 10^{-7}$
L_π	0.999 (74) $\times 10^{-10}$	

from Ramsay and Sarre's (*4*) values, especially for the B_π constant. This is a consequence of their treatment of the relatively large Λ doubling in the $c^1\Pi$ state with equal upward and downward shifts for levels having positive or negative symmetry. The value for the band origin depends of course on the absolute calibration of the I_2 atlas (*22*), where an absolute error of 60 MHz had been claimed (*23*). We choose not to enlarge our experimental errors with this calibration error of the I_2 standard. For the determination of accurate rotational constants only the relative errors in the I_2 lines, i.e., 0.0005 cm^{-1} or 15 MHz, is relevant.

5. CONCLUSION

The molecular beam apparatus, with its coaxial microwave cavity for the NH production is a powerful tool for spectroscopic studies of molecules in various electronic states, including metastable state radicals. The very narrow molecular beam together with a tunable narrowband UV source allow for high-resolution studies of these molecules. As far as the NH molecule is concerned besides the $X^3\Sigma^-$ ground state and the metastable $a^1\Delta$ state, the other $b^1\Sigma^+$ metastable state might be detected in the same setup with available narrowband blue dye lasers in the $c^1\Pi \leftarrow b^1\Sigma^+$ transition at $\lambda = 450$ nm. The radiative lifetime of the NH($b^1\Sigma^+$) state is 53 msec according to Blumenstein *et al.* (*24*), long enough for detection in a molecular beam.

With the present investigation the hyperfine constants in four electronic states of NH, the $X^3\Sigma^-$, $a^1\Delta$, $A^3\Pi$, and $c^1\Pi$ are known within 1%. This opens the possibility to test ab initio calculations on this relatively simple molecule.

From relative frequency measurements we obtained for the first time an accurate constant for the Λ doubling in a Δ state. In the past Caton and Douglas (*25*) determined a Λ-doubling parameter for the $BF(^1\Delta)$ molecule and recently Brazier and Brown (*26*) did the same for CH($^2\Delta$), but with a much lower accuracy.

The absolute frequency measurements enabled us to improve the values for the rotational constants by a factor of 4. We were limited by the accuracy in the calibration of the I_2 atlas and particularly by the width ($\sim$1.5 GHz) of the I_2 lines as measured in an absorption cell. By the use of a better absolute wavelength calibration standard, it should be possible to gain another factor of 10 in the accuracy. We hope that in the future the accuracy of the relative frequency measurements also can be further improved by the use of a better temperature-stabilized interferometer with a smaller free spectral range (75 MHz).

RECEIVED: February 11, 1985

REFERENCES

1. R. W. B. PEARSE, *Proc. R. Soc. A* **143,** 112–123 (1934).
2. G H. DIEKE AND R. W. BLUE, *Phys. Rev.* **45,** 395–400 (1934).
3. G. NAKAMURA AND T. SHIDEI, *Japan. J. Phys.* **10,** 5–10 (1934).
4. D. A. RAMSAY AND P. J. SARRE, *J. Mol. Spectrosc.* **93** 445–446 (1982).
5. W. R. M. GRAHAM AND H. LEW, *Canad. J. Phys.* **56,** 85–99 (1978).
6. G. KRISHNAMURTY AND N. A. NARASINHAM, *J. Mol. Spectrosc.* **29,** 410–414 (1969).
7. A. GILLES, J. MASANET, AND C. VERMEIL, *Chem. Phys. Lett.* **25,** 346–347 (1974).
8. F. ROHRER AND F. STUHL, *Chem. Phys. Lett.* **111,** 234–347 (1984).
9. K. H. WELGE, *J. Chem. Phys.* **45,** 4373–4374 (1966).

10. H. OKABE, *J. Chem. Phys.* **49,** 2726–2733 (1968).
11. Z. G. PIPER, R. H. KRECH, AND R. L. TAYLOR, *J. Chem. Phys.* **73,** 791–800 (1980).
12. O. KAJIMOTO AND T. FUENO, *Chem. Phys. Lett.* **80,** 484–487 (1981).
13. W. UBACHS, J. J. TER MEULEN, AND A. DYMANUS, *Canad. J. Phys.* **62,** 1374–1391 (1984).
14. W. R. ANDERSON AND D. R. CROSLEY, *Chem. Phys. Lett.* **62,** 275–278 (1979); P. W. FAIRCHILD, G. P. SMITH, D. R. CROSLEY, AND J. B. JEFFRIES, *Chem. Phys. Lett.* **107,** 181–186 (1984).
15. E. FINK AND H. WELGE, *Z. Naturforsch.* **19a,** 1193–1201 (1964).
16. W. H. SMITH AND H. S. LISZT, *JQRT* **11,** 45–54 (1971).
17. J. R. MCDONALD, R. G. MILLER, AND A. P. BARANOVSKI, *Chem. Phys. Lett.* **51,** 57–60 (1977).
18. R. A. FROSCH AND H. M. FOLEY, *Phys. Rev.* **88,** 1337–1349 (1952).
19. F. L. WHITTAKER, *J. Phys. B.* **1,** 977–982 (1968).
20. R. W. LUNT, R. W. B. PEARSE, AND E. C. W. SMITH, *Proc. R. Soc A***151,** 602–609 (1935).
21. R. W. LUNT, R. W. B. PEARSE, AND E. C. W. SMITH, *Proc. R. Soc A***155,** 173–182 (1936).
22. S. GERSTENKORN AND P. LUC, "Atlas du spectroscopie d'absorption de la molecule d'iode," CNRS, Paris, 1978.
23. S. GERSTENKORN AND P. LUC, *Rev. Phys. Appl.* **14,** 791–794 (1979).
24. U. BLUMENSTEIN, F. ROHRER, AND F. STUHL, *Chem. Phys. Lett.* **107,** 347–350 (1984).
25. R. B. CATON AND A. E. DOUGLAS, *Canad. J. Phys.* **48,** 432–452 (1970).
26. C. R. BRAZIER AND J. M. BROWN, *Canad. J. Phys.* **62,** 1563–1578 (1984).